Electrically driven thermal light emission from individual single-walled carbon nanotubes

DAVID MANN[1], Y. K. KATO[1], ANIKA KINKHABWALA[1], ERIC POP[1,2], JIEN CAO[1], XINRAN WANG[1], LI ZHANG[1], QIAN WANG[1], JING GUO[3] AND HONGJIE DAI[1]*

[1]Department of Chemistry and Laboratory for Advanced Materials, Stanford University, Stanford, California 94305, USA
[2]Intel Corporation, Santa Clara, 2200 Mission College Boulevard, California 95054, USA
[3]Department of Electrical and Computer Engineering, University of Florida, Gainesville, Florida 32611, USA
*e-mail: hdai@stanford.edu

Published online: 3 January 2007; doi:10.1038/nnano.2006.169

Light emission from nanostructures exhibits rich quantum effects and has broad applications. Single-walled carbon nanotubes (SWNTs) are one-dimensional metals or semiconductors in which large numbers of electronic states in narrow energy ranges, known as van Hove singularities, can lead to strong spectral transitions[1,2]. Photoluminescence and electroluminescence involving interband transitions and excitons have been observed in semiconducting SWNTs[3–9], but are not expected in metallic tubes owing to non-radiative relaxations. Here, we show that, under low bias voltages, a suspended quasi-metallic SWNT (QM-SWNT) emits light owing to Joule heating, displaying strong peaks in the visible and infrared, corresponding to interband transitions. This is a result of thermal light emission in a one-dimensional system, in stark contrast with featureless blackbody-like emission observed in large bundles of SWNTs or multiwalled nanotubes[10–12]. This allows for probing of the electronic temperature and non-equilibrium hot optical phonons in Joule-heated QM-SWNTs.

We investigated electrically driven thermal light emission of individual QM-SWNTs in both the visible and infrared (wavelength $\lambda = 500-2{,}100$ nm; see experimental details in Supplementary Information), in a wider spectral window than previously explored for electroluminescence of nanotubes. We fabricated suspended and non-suspended SWNT (diameter $d \approx 2-4$ nm) devices with tube length $L \approx 2-10$ μm (Fig. 1a, c insets), as described previously[13–15]. QM-SWNTs were identified as those exhibiting weak source–drain current (I_{ds}) dependence (due to small bandgaps of tens of meV (refs 14,16) on gate-voltage (V_{gs}) with $I_{ds}(\max)/I_{ds}(\min) < 10$ (at bias $V_{ds} = 10$ mV), across the V_{gs} range (Fig. 1a). On substrate, QM-SWNTs show current saturation near 20 μA at high bias, but suspended ones exhibit negative differential conductance (that is, reduced currents at higher biases) and much lower maximum current <10 μA (Fig. 1b) due to Joule heating and electron scattering by hot optical phonons caused by slow heat dissipation in the suspended SWNTs[15].

We observed light emission from suspended QM-SWNTs (in the on state under a high negative V_{gs}, with the device kept in Ar) beginning at low V_{ds}, with pronounced peaks in the spectra (Figs 1c, 2a, b). We measured the visible emission characteristics of the suspended and on-substrate sections of several QM-SWNTs (Fig. 1c) and observed that the onset of detectable visible light for suspended QM-SWNT devices began as low as $V_{ds} = 0.9$ V (always in the negative differential conductance region in $I_{ds}-V_{ds}$ as in Fig. 1b), but the visible emission for on-substrate SWNTs was not measurable until $V_{ds} > 5$ V. For several long (10 μm) suspended QM-SWNTs, we spatially resolved light emission and found that the location of the brightest spot was always near the centre (Fig. 1d) and remained stationary at various V_{ds} and V_{gs}.

We investigated light emission from ten suspended (all in Ar) QM-SWNTs (Fig. 2). All QM-SWNTs exhibited spectral peaks and the peak positions varied (Fig. 2a,b). In SWNTs, electronic transitions between the van Hove singularities are dipole-allowed (denoted as E_{nn} transitions)[17]. We attribute the observed peaks to optical emission (highly polarized along the tube axis; Fig. 2b inset) from E_{11} (infrared) and E_{22} (visible or near infrared) transitions (Fig. 2c) of QM-SWNTs. Lorentzian fitting is used to determine the peak locations of E_{11} and E_{22}. We find reasonable agreement with simple tight-binding predicted E_{11} and E_{22} values[18] (~1 : 2 ratio) (Fig. 2d) for QM-SWNTs with $d \approx 2.8-4$ nm (d was measured by atomic force microscopy over the on-substrate portion of the nanotubes).

To understand the light emission in QM-SWNTs, we note that the negative differential conductance in the $I_{ds}-V_{ds}$ of suspended QM-SWNTs is indicative of significant self-heating and electron scattering by hot optical phonons[15]. The slow decay and long lifetimes of optical phonons in suspended SWNTs lead to high non-equilibrium optical phonon population and temperature (T_{op}), causing significant electron heating ($T_e \approx T_{op}$) well above the temperature of the SWNT lattice[15,19]. Analysis of the negative differential conductance region of the $I_{ds}-V_{ds}$ curve of a ~2 μm suspended QM-SWNT by the hot phonon model[15,19] leads to an estimated $T_e \approx T_{op} \approx 1{,}200$ K at $V_{ds} \approx 1.3$ V. This heating gives rise to a thermal distribution of electrons and holes with appreciable populations at the van Hove singularities in QM-SWNTs (Fig. 2c). These carriers can then radiatively recombine to

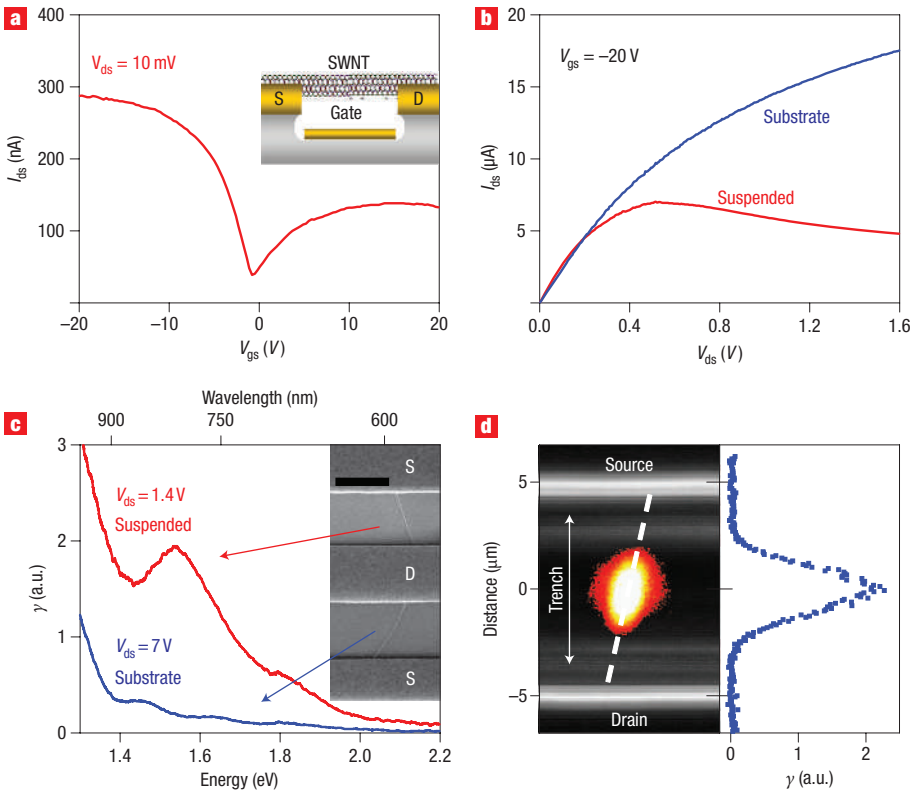

Figure 1 Visible thermal light emission of quasi-metallic SWNTs. a, Current versus gate voltage $I_{ds}-V_{gs}$ curve for a 2-μm-long suspended QM-SWNT device schematically shown in the inset (S, source; D, drain). **b**, Current versus bias $I_{ds}-V_{ds}$ characteristics of the SWNT in **a** (showing negative difference conductance), together with those of the non-suspended portion of the same tube. **c**, Visible emission spectra for the suspended and non-suspended portion of the QM-SWNT recorded at low and high bias V_{ds}, respectively ($V_{ds} = 1.4$ V, $I_{ds} = 5$ μA; $V_{ds} = 7$ V, $I_{ds} = 21$ μA). The inset shows a scanning electron microscopy image (scale bar is 2 μm) of the device with suspended and on-substrate SWNT portions bridging electrodes. **d**, Visible confocal image of a 10-μm suspended QM-SWNT at $V_{ds} = 1.9$ V ($I \approx 3$ μA) collected by a silicon avalanche photodetector superimposed on a dark-field optical image (the brightest horizontal lines mark the edge of the electrodes). The strongest light emission is seen at the centre of the suspended tube (approximate location traced by the dashed line). Right panel: γ line cut (total photon counts) along the tube length. The resolution of this measurement is nearly diffraction limited (~1 μm).

produce E_{11} and E_{22} emission peaks, thus producing distinct spectral features rather than a featureless blackbody spectrum. Note that excitons may play a role in metallic and QM-SWNTs, but the effect should be smaller in our case than in semiconducting SWNTs owing to large $d \approx 2-4$ nm QM-SWNTs used with low exciton binding energies[20] relative to the high T_e involved. The effect is difficult to discern from our spectra with broad peaks caused by significant heating.

This thermal light emission model is consistent with the observed emission photon energy exceeding the bias-voltage injection energy eV_{ds} (emission well above $eV_{ds} = 1.4$ eV is seen in Fig. 1c). It is also consistent with the drastic difference in light emission between the suspended and on-substrate portions of a SWNT (Fig. 1c), because self-heating of the latter is much lower owing to efficient thermal dissipation and optical phonons relaxing into the substrate[15,21]. In fact, in ambient air without the protection of Ar flow, our suspended SWNTs break down at sustained biases $V_{ds} \approx 1.5-2$ V (see Supplementary Information, Fig. S1) as a result of oxidation as their lattice temperature approaches ~800 K (ref. 22). The thermal light emission model is also consistent with the fact that light emission is brightest at the centre of the suspended QM-SWNTs (Fig. 1d) where a parabolic temperature profile peaks[15]. This differs from previous spatially resolved electroluminescence in semiconducting-SWNTs in which emission was observed at the suspended trench edge attributed to impact excitation and exciton recombination[7], and the mobile emission spot seen as a result of ambipolar carrier injection[5]. We carried out theoretical modelling (see Methods section) to fit the experimental spectra (Fig. 3a & 3c) and extract electron temperatures by spectra fitting in the visible region, and the results were close to the optical phonon temperature ($T_e \sim T_{op}$) derived from the hot phonon model (Fig. 3b, left axis)[15,19]. Note that our model is mainly used to fit the exponential emission tail in the visible for extracting electron temperature and is not intended to precisely fit the peak positions.

Several features in our spectra are not well understood. First, $E_{11}:E_{22} \sim 1:1.7-2$ has been observed for semiconducting-SWNTs by photoluminescence experiments[23,24]. In our case of QM-SWNT thermal light emission, in which we do not consider excitonic effects, we expect $E_{11}:E_{22} \approx 1:2$, but deviations from this ratio were observed (Fig. 2d). One possible cause is a significant heating effect on the nanotube structure and in turn electronic structure. Some of our QM-SWNTs exhibited unexplained peaks (for example, in the red curve of Fig. 2a) between E_{11} and E_{22}. Possible explanations for this include phonon-assisted transitions, inter-band transitions (such as E_{12}, for which theoretical work has suggested perpendicular polarization and intensity up to a ~1/5–1/3 of E_{nn} transitions[25]),

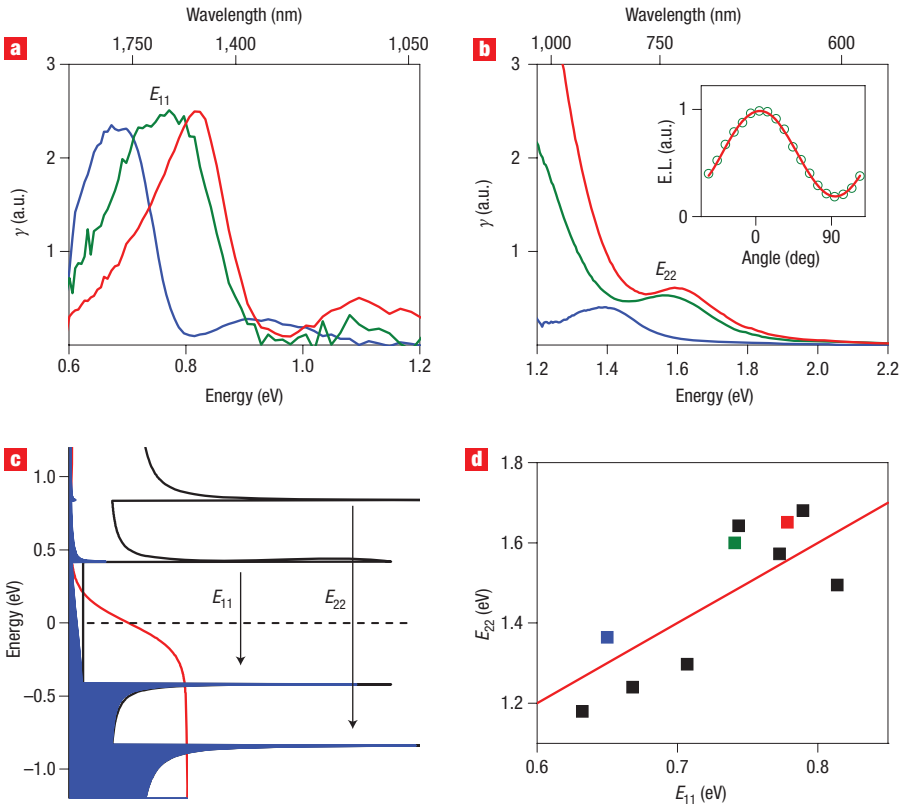

Figure 2 Thermal light emission of suspended metallic SWNTs with E_{11} and E_{22} peaks. a, Light emission spectra (scaled for readability) in the infrared for three independent 2-μm-long QM-SWNTs (red, green and blue) at $V_{gs} = -20$ V and $V_{ds} = 1.4$, 1.1 and 1.3 V, respectively ($I_{ds} = 6.35$, 5.13, 5.95 μA). **b**, Corresponding light emission spectra for the three tubes in **a** in the visible at $V_{gs} = -20$ V and $V_{ds} = 1.5$, 1.3, 1.5 V ($I_{ds} = 6.15$, 4.78, 5.7 μA), respectively. In the inset, the symbols are measured photon counts for emission polarized at various angles relative to the tube axis. The solid line is a $\cos^2$ fit. **c**, Illustration of the thermal light emission mechanism in a $(n,m) = (24,21)$ QM-SWNT (with $d \approx 3$ nm, $E_{11} \approx 0.8$ eV, $E_{22} \approx 1.6$ eV as for the tube in **a** and **b** with red curves). The curve on the blue region corresponds to the electron population at various energies calculated by multiplying the density-of-states (black line) and the Fermi–Dirac distribution (red line) at $T_e \approx 1{,}200$ K. The finite populations at the first and second van Hove singularities are responsible for E_{11} and E_{22} optical emission and depend on T_e and energy exponentially. **d**, E_{11} versus E_{22} peak locations from ten suspended QM-SWNT devices determined from their visible and infrared spectra. The red line corresponds to $E_{22} = 2E_{11}$ from the simple tight-binding approximation. The peaks were determined using a Lorentzian curve fit. As a result, some of the devices showing asymmetric peaks had some offset due to an imperfect fit.

and perhaps emission from states due to defects along the relatively long tubes. These possibilities require further investigation. We calculated the effect of trigonal warping[26] on our spectra and found the effect to be inconsequential in this diameter range ($d \approx 2.8$–4 nm), given the breadth of the measured emission peaks (>100 meV).

For the SWNT in Fig. 3c we analysed the peak width (full-width half maximum σ of ~130 meV) as a function of bias by fitting several spectra ($V_{ds} = 0.7$–1.2 V). As V_{ds} and thus T_e increase, the emission peak is expected to widen from increased thermal and lifetime broadening effects. Indeed, we observed a change in peak width over the bias range (Fig. 3c). The apparent peak widths correspond to effective total lifetimes of $\tau_{TOT} \approx$ 10–14 fs, including all scattering mechanisms (Fig. 3d, left axis). By using the calculated T_{op} (and the corresponding Bose–Einstein optical phonon occupation number) from the hot phonon model[15,19], we determined an electron–phonon scattering lifetime τ_{e-op} of ~15–18 fs (Fig. 3d, right axis), about 50% greater than τ_{TOT}. This suggests that only a portion of τ_{TOT} is due to electron–phonon scattering, with additional broadening likely due to other mechanisms, such as electron–electron scattering.

Finally, we carried out light emission measurements of QM-SWNTs as a function of bias V_{ds} and gate-voltage V_{gs} (Fig. 4). At a fixed bias V_{ds}, the infrared light emission γ (down to 0.57 eV) under various V_{gs} scaled exponentially with current or power ($P = I_{ds}V_{ds}$) (Fig. 4a), as increases in the latter caused higher T_e. Current modulation by V_{gs} (Fig. 4b; also Fig. 1a) was due to the existence of small bandgaps (of the order of tens of meV) in the QM-SWNTs[13–16]. By simultaneously measuring light emission γ and power P versus V_{ds} and V_{gs} (Fig. 4c and d, respectively), we observed that the exponential dependence of γ on P held across the entire V_{gs} and V_{ds} two-dimensional space.

Figure 4a has striking similarities to the data presented previously[7]. Although Chen *et al.* attribute this to impact excitation and recombination of free carriers and excitons[7], we rule out impact excitation as the cause of light emission in our devices owing to the observation of photons of greater energy than the applied field ($E_{photon} > eV_{ds}$) (Fig. 1c, red curve, and Fig. 3a). Additionally, we do not expect appreciable light emission from impact excitation as a result of non-radiative relaxation of excited carriers in QM-SWNTs[20]. We have also measured light emission of suspended semiconducting SWNTs and found

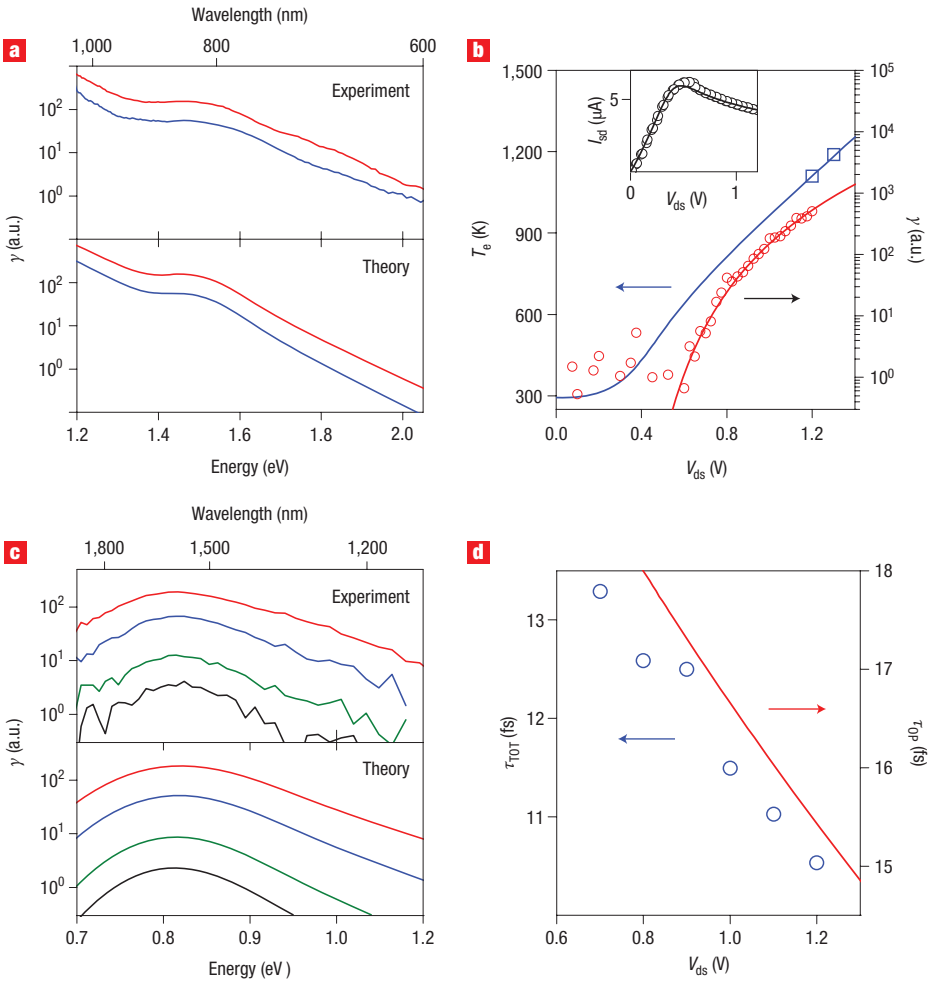

Figure 3 Thermal light emission spectra of a 2.9-μm-long suspended QM-SWNT compared with theory. a, The top panel shows visible spectra of a 2.9-μm-long suspended QM-SWNT at two biases $V_{ds} = 1.2$ V (blue) and 1.3 V (red). The lower panel shows spectra calculated for a $d \approx 3$ nm SWNT with $E_{11} \approx 0.8$ eV and $E_{22} \approx 1.6$ eV using equation (1) (see Methods). Several $d \approx 3$ nm SWNTs, such as (24,21) and (28,16), have similar E_{11} and E_{22}, making it not possible to uniquely determine (n,m). **b**, Left axis: Electron temperature T_e ($\sim T_{op}$) versus bias (blue line) derived by fitting $I_{ds}-V_{ds}$ data (symbols in inset) using the hot phonon model[15,19]. Blue squares are T_e extracted from fitting visible thermal light emission spectra (see Methods) in **a** for the two biases. Right axis: Measured γ versus bias in the infrared region (red symbols) and computed γ (red line) based on T_e derived from the $I_{ds}-V_{ds}$ model[15,19]. **c**, Thermal light emission spectra in the infrared region for the SWNT at $V_{ds} = 0.7$ (black), 0.8 (green), 1.0 (blue) and 1.2 V (red) (top panel). The lower panel shows spectra calculated using equation (1) and T_e at corresponding biases from **b**. Note that a more precise theoretical treatment should include any exciton effects in our $d \approx 2-4$ nm QM-SWNTs. The exciton binding energies for large-diameter QM-SWNTs are unknown, but should be smaller than the ~80 meV theoretically expected for a $d \approx 0.5$ nm QM-SWNT[27]. The effect may cause a shift in the emission peak positions, but the shift will be small compared to the large thermal light emission peak width (~130 meV). **d**, Left axis: estimated hot-electron lifetime (τ_{TOT}) at various biases. Right axis: calculated electron–optical phonon scattering time at various biases at corresponding temperatures obtained from $I_{ds}-V_{ds}$ analysis.

that thermal effects also occur in semiconducting tubes (see Supplementary Information, Fig. S2). The data suggest that thermal heating may play a role in other electroluminescence measurements of semiconducting SWNTs[3–9] where similar or higher powers than those reported here are dissipated in the devices.

Our measurement reveals the high-temperature optoelectronic properties of quasi-metallic SWNTs. By exploiting SWNTs of specific diameters, one can produce thermal light emission peaked at a desired wavelength, from the visible to the infrared, which is useful in optoelectronics for telecommunications in the 1.3–1.5 μm range. Although thermal light emission of bulk materials has been extensively studied, our result, revealing drastic spectra peaks for SWNTs, underlines the importance of examining electronic heating and emission in novel nanomaterials.

METHODS

EXPERIMENTAL DETAILS

Fabrication of devices, methods for ensuring single tubes, light emission spectra and spatially resolved emission and electrical measurements are described in the Supplementary Information.

THEORETICAL MODELLING OF THERMAL LIGHT EMISSION SPECTRA OF QM-SWNTs

We use the tight-binding approximation to calculate the approximate joint density of states $D_j(E) = D(E/2)/2$ (where E is the transition energy and D is the density of states)[18] for a SWNT of a certain diameter d, and

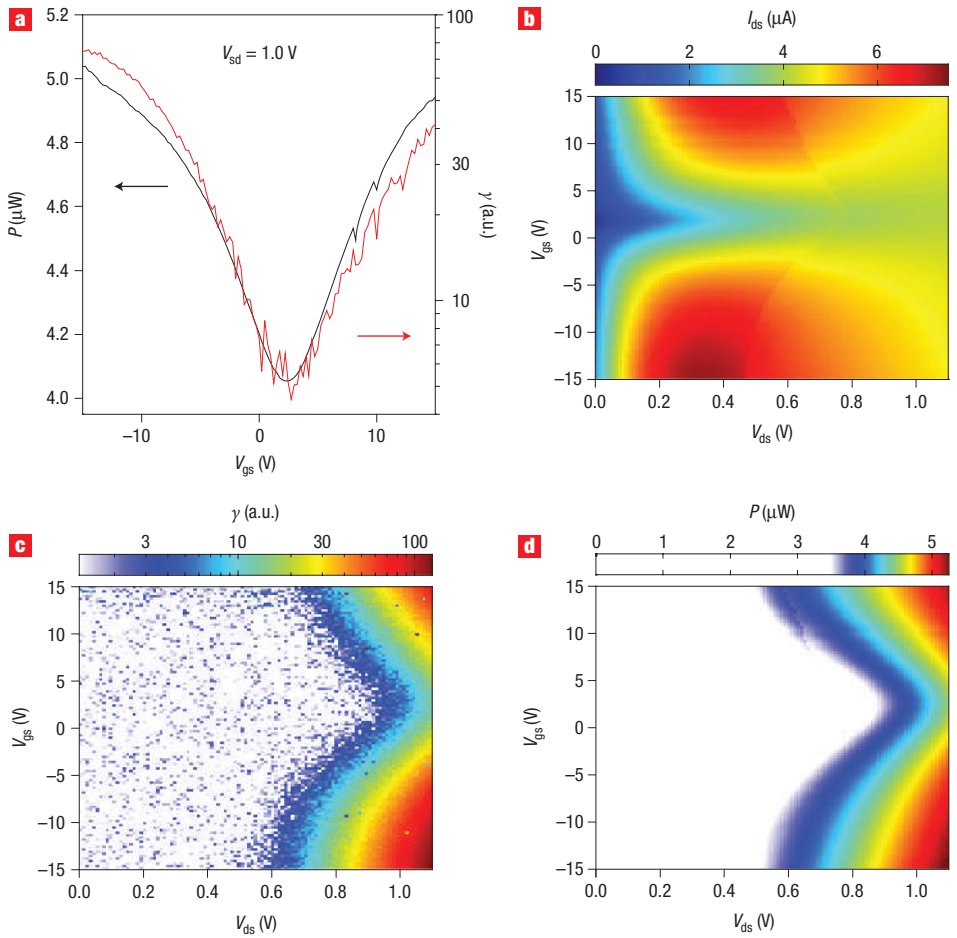

Figure 4 Thermal light emission of suspended QM-SWNTs exhibits exponential dependence on power dissipation in the devices. a, Total power dissipation $P(=I_{ds}V_{ds})$ versus V_{gs} for a typical QM-SWNT device at $V_{ds}=1$ V (black line, left axis in linear scale) and corresponding emission (total photon count in log scale) versus V_{gs} in the infrared (red line, right axis). The electrical contact resistance is always an order of magnitude less than the suspended SWNT resistance at high bias. Power dissipation due to contact resistance was not excluded from *P*. **b**, I_{ds} map (colour scale bar on top) at various V_{ds} and V_{gs}, showing the evolution of $I_{ds}-V_{ds}$ versus V_{gs}. **c**, Thermal light emission (γ) map (top: colour scale in log) in the infrared region at various V_{ds} and V_{gs}. **d**, Power dissipation map *P* (top: colour scale bar in linear scale) calculated by $P=I_{ds}V_{ds}$ from **b** at various V_{ds} and V_{gs}. The close resemblance between the thermal light emission map in the log scale and power dissipation map in the linear scale strongly suggests that light emission scales exponentially with power and supports the thermal light emission model.

introduce broadening of the D_J by convolving it with a function *B* (either gaussian or Lorentzian)[28]

$$D_J^B(E)=\int_{-\infty}^{+\infty} dE'\cdot D_J(E')\cdot B(E-E',\sigma),$$

where σ is the broadening width (due to the finite lifetime of carriers scattered by phonons and other mechanisms) and is used as a fitting parameter. It is important to note that D_J does not include the metallic electronic band, because the dipole transition matrix element is zero for that band[29]. As an approximation (without including exciton effects for the large-diameter QM-SWNTs used in the current work), we calculated the emission spectrum by[30]

$$S(E)=\frac{1}{\tau(E)}D_J(E)f_0[E_C(k)-F_n]\left\{1-f_0\left[E_V(k)-F_p\right]\right\}, \qquad (1)$$

where $S(E)$ is the photon count (~light intensity), $E=E_C(k)-E_V(k)$ is the emitted photon energy, $D_J(E)$ is the joint density-of-states, $f_0(E)$ is the Fermi–Dirac distribution at high T_e (resulting from self-heating) and $1/\tau(E)$ is the transition probability. $E_C(k)=-E_V(k)$ if the middle of the bandgap is defined as the energy zero, because the conduction and valence bands of SWNTs are symmetric, and we assume that the electron and hole quasi-Fermi levels $F_n\approx F_p\approx 0$ under all experimental gate voltages because the nanotube is quasi-metallic and the gate efficiency factor is small (~0.01; refs 13–15). (Fermi level modulation by gate voltages only leads to a variation of <20% in the product of the electron and hole Fermi–Dirac population terms in equation (1).) The emission rate $1/\tau(E)=2\pi/\hbar(q/m_0p_{CV}A)^2(2/3D_{ph}(E))$ depends on the momentum matrix element p_{CV}, the magnitude of the vector potential *A*, and the photon density of states $D_{ph}(E)$, and we assume that it is energy-independent for simplicity[30]. For three-dimensional isotropic (blackbody) photons, $D_{ph}\propto\omega^2$ $(E=h\omega)$, and $1/\tau(E)\sim p_{CV}^2\omega\sim r_{CV}^2\omega^3$, where the dipole matrix element $r_{CV}=p_{CV}/(im_0\omega)$ and *i* is the imaginary unit. In a quasi one-dimensional SWNT, the momentum matrix element p_{CV} slightly decreases with energy[29]. The energy dependence of the emission spectrum in equation (1) is then dominated by the Fermi–Dirac distribution terms in an exponential manner. From ~1.2 eV to 2.0 eV in the visible range in which our model fitting is carried out for electron temperature extraction, $1/\tau(E)$ is computed using $\sim{p_{CV}}^2\omega$ varies by a factor of <2, but the product of the Fermi–Dirac distribution terms varies by more than 4 orders of magnitude at $T_e=1{,}000$ K.

Using our model with gaussian broadening, we obtained excellent fitting of the experimental visible spectra (Fig. 3a) and were able to extract T_e at various V_{ds} (square symbols in Fig. 3b). The emission spectrum in the visible essentially exhibits an exponential decay ($\sim e^{-E/k_BT_e}$ due to the Fermi–Dirac

distributions in equation (1)) into the high-energy end, with a superimposing hump at ~1.6 eV corresponding to the E_{22} transition (Fig. 3a). Thus the visible spectrum of suspended QM-SWNTs allows for an experimental determination of T_e ($\sim T_{op}$) for individual SWNTs under Joule heating at various V_{ds}. Under higher V_{ds}, a suspended SWNT exhibits more Joule heating and higher T_e (Fig. 3b, left axis), and thus an exponential increase in light emission (see bias-dependent spectra in Fig. 3a, c and Fig. 3b, right axis). Importantly, we found that the extracted T_e (squares in Fig. 3b) from the emission spectra agree well with those obtained (Fig. 3b, blue line) by fitting $I_{ds}-V_{ds}$ curves (Fig. 3b inset) using the hot phonon model[15,19].

The emission spectra of suspended QM-SWNTs in the lower energy infrared regime were dominated by the E_{11} peak (Figs 2a and 3c). This supports our assumption for the model where the transitions within the metallic band are forbidden[29], because otherwise an exponentially increasing emission would exist on the lower energy side of the E_{11} peak. It is interesting that thermal light emission spectra provide insights into the magnitudes of the optical transition matrix elements, but the lack of an exponential slope causes difficulty in extracting T_e by spectral analysis in the infrared region. Instead, by using the calculated temperatures from the $I_{ds}-V_{ds}$ fits, Lorentzian broadening, and allowing only the width σ to vary (after fixing the other parameters by fitting one spectrum), we modelled the infrared spectra with excellent agreement with experiment for the SWNT in Fig. 3c. This agreement suggests that contrasting SWNT emission spectra in the infrared region with blackbody is not sufficient to exclude the possibility of thermal emission, as carried out in a recent work[8]. The total photon counts γ in the infrared (Fig. 3b, red line) can be estimated as $\gamma(T_e) \sim Ae^{-E/k_B T_e}$ at various V_{ds} (and in turn various T_e) with $E \sim 0.8$ eV $\sim E_{11}$ (photon energy of the peak in Fig. 3c), in agreement with the measured results (Fig. 3b, red symbols).

Received 4 August 2006; accepted 21 November 2006; published 3 January 2007.

References

1. Dresselhaus, M. & Dai, H. (eds) MRS 2004 Carbon Nanotube Special Issue **29** (2004).
2. Saito, R., Fujita, M., Dresselhaus, G. & Dresselhaus, M. S. Electronic structure of graphene tubules based on C_{60}. *Phys. Rev. B* **46,** 1804–1811 (1992).
3. O'Connell, M. J. *et al.* Band gap fluorescence from individual single-walled carbon nanotubes. *Science* **297,** 593–596 (2002).
4. Lefebvre, J., Homma, Y. & Finnie, P. Bright band gap photoluminescence from unprocessed single-walled carbon nanotubes. *Phys. Rev. Lett.* **90,** 217401 (2003).
5. Freitag, M. *et al.* Mobile ambipolar domain in carbon-nanotube infrared emitters. *Phys. Rev. Lett.* **93,** 076803 (2004).
6. Freitag, M. *et al.* Hot carrier electroluminescence from a single carbon nanotube. *Nano Lett.* **4,** 1063–1066 (2004).
7. Chen, J. *et al.* Bright infrared emission from electrically induced excitons in carbon nanotubes. *Science* **310,** 1171–1174 (2005).
8. Marty, L. *et al.* Exciton formation and annihilation during 1D impact excitation of carbon nanotubes. *Phys. Rev. Lett.* **96,** 136803 (2006).
9. Misewich, J. A. *et al.* Electrically induced optical emission from a carbon nanotube FET. *Science* **300,** 783–786 (2003).
10. Sveningsson, M., Jonsson, M., Nerushev, O. A., Rohmund, F. & Campbell, E. E. B. Blackbody radiation from resistively heated multiwalled carbon nanotubes during field emission. *Appl. Phys. Lett.* **81,** 1095–1097 (2002).
11. Wei, J. Q., Zhu, H. W., Wu, D. H. & Wei, B. Q. Carbon nanotube filaments in household light bulbs. *Appl. Phys. Lett.* **84,** 4869–4871 (2004).
12. Li, P. *et al.* Polarized incandescent light emission from carbon nanotubes. *Appl. Phys. Lett.* **82,** 1763–1765 (2003).
13. Cao, H., Wang, Q., Wang, D. W. & Dai, H. J. Suspended carbon nanotube quantum wires with two gates. *Small* **1,** 138–141 (2005).
14. Cao, J., Wang, Q. & Dai, H. Electron transport in very clean, as-grown suspended carbon nanotubes. *Nature Mater.* **4,** 745–749 (2005).
15. Pop, E. *et al.* Negative differential conductance and hot phonons in suspended nanotube molecular wires. *Phys. Rev. Lett.* **95,** 155505 (2005).
16. Zhou, C., Kong, J. & Dai, H. Intrinsic electrical properties of single-walled carbon nanotubes with small band gaps. *Phys. Rev. Lett.* **84,** 5604–5607 (2000).
17. Ichida, M. *et al.* Coulomb effects on the fundamental optical transition in semiconducting single-walled carbon nanotubes: Divergent behavior in the small-diameter limit. *Phys. Rev. B* **65,** 241407 (2002).
18. Mintmire, J. W. & White, C. T. Universal density of states for carbon nanotubes. *Phys. Rev. Lett.* **81,** 2506–2509 (1998).
19. Mann, D. *et al.* Thermally and molecularly stimulated relaxation of hot phonons in suspended carbon nanotubes. *J. Phys. Chem. B* **110,** 1502–1505 (2006).
20. Ando, T. Excitons in carbon nanotubes. *J. Phys. Soc. Jpn* **66,** 1066–1073 (1997).
21. Pop, E., Mann, D., Reifenberg, J., Goodson, K. E. & Dai, H. J. in *Intl Electron Devices Meeting (IEDM)* 253–256 (Washington DC, 2005).
22. Hata, K. *et al.* Water-assisted highly efficient synthesis of impurity-free single-walled carbon nanotubes. *Science* **306,** 1362–1364 (2004).
23. Bachilo, S. M. *et al.* Structure-assigned optical spectra of single-walled carbon nanotubes. *Science* **298,** 2361–2366 (2002).
24. Weisman, R. B. & Bachilo, S. M. Dependence of optical transition energies on structure for single-walled carbon nanotubes in aqueous suspension: An empirical Kataura plot. *Nano Lett.* **3,** 1235–1238 (2003).
25. Milosevic, I., Vukovic, T., Dmitrovic, S. & Damnjanovic, M. Polarized optical absorption in carbon nanotubes: A symmetry-based approach. *Phys. Rev. B* **67,** 165418 (2003).
26. Saito, R., Dresselhaus, G. & Dresselhaus, M. S. Trigonal warping effect of carbon nanotubes. *Phys. Rev. B* **61,** 2981–2990 (2000).
27. Spataru, C. D., Ismail-Beigi, S., Benedict, L. X. & Louie, S. G. Excitonic effects and optical spectra of single-walled carbon nanotubes, *Phys. Rev. Lett.* **92,** 077402 (2004).
28. Hertel, T. & Moos, G. Influence of excited electron lifetimes on the electronic structure of carbon nanotubes. *Chem. Phys. Lett.* **320,** 359–364 (2000).
29. Goupalov, S. V. Optical transitions in carbon nanotubes. *Phys. Rev. B* **72,** 195403–195407 (2005).
30. Rosencher, E. & Vinter, B. *Optoelectronics* (Cambridge Univ. Press, Cambridge, UK, 2002).

Acknowledgements

We thank W. E. Moerner for use of the confocal optical setup. This work was supported in part by MARCO MSD Focus Center and a NSF-NIRT.
Correspondence and request for materials should be addressed to H.D.
Supplementary information accompanies this paper on www.nature.com/naturenanotechnology.

Author contributions

H.D., D.M. and Y.K. conceived and designed the experiments. D.M., Y.K., A.K., E.P., J.C, X.W., L.Z., Q.W. and J.G. performed the experiments and analysed the data. H.D., D.M. and Y.K. co-wrote the manuscript. All authors discussed the results and commented on the manuscript.

Competing financial interests

The authors declare that they have no competing financial interests.